Research Square

Preprints are preliminary reports that have not undergone peer review.
They should not be considered conclusive, used to inform clinical practice,
or referenced by the media as validated information.

Ecological connectivity in a protected area network under deep-sea mining

Molly James

moja@pml.ac.uk

Plymouth Marine Laboratory https://orcid.org/0000-0002-3097-0812

Amelia Bridges

University of Plymouth https://orcid.org/0000-0002-1422-9637

Daniel Jones

National Oceanography Centre Southampton https://orcid.org/0000-0001-5218-1649

Charlotte Clubley

Aarhus University

Antony Knights

University College Cork

Danielle de Jonge

Scottish Association for Marine Science (SAMS) https://orcid.org/0000-0002-4093-2721

Kerry Howell

Plymouth Marine Laboratory

Biological Sciences - Article

Keywords:

Posted Date: September 29th, 2025

DOI: https://doi.org/10.21203/rs.3.rs-7590015/v1

License: This work is licensed under a Creative Commons Attribution 4.0 International License.
Read Full License

Additional Declarations: There is **NO** Competing Interest.

Version of Record: A version of this preprint was published at Nature Ecology & Evolution on October 23rd, 2026. See the published version at https://doi.org/10.1038/s41559-026-03172-5.

Ecological connectivity in the protected area network under deep-sea mining

Molly K. James[1*], Amelia E.H. Bridges[2], Daniel O. B. Jones[3], Charlotte H. Clubley[4], Antony M. Knights[5], Daniëlle de Jonge[6] and Kerry L. Howell[1,2]

1. Plymouth Marine Laboratory, Prospect Place, Plymouth, Devon, UK. PL1 3DH
2. School of Biological and Marine Sciences, University of Plymouth, Drake Circus, Plymouth, Devon, UK. PL4 8AA
3. National Oceanography Centre, European Way, Southampton, UK. SO14 3ZH
4. Aarhus University, Department of Ecoscience, Frederiksborgvej 399, 4000 Roskilde, Denmark.
5. School of Biological, Earth and Environmental Sciences, University College Cork, Distillery Fields, Cork, Ireland
6. Joint Nature Conservation Committee, Inverdee House, Baxter Street, Aberdeen, AB11 9QA, UK.

*Corresponding author
Corresponding author email: moja@pml.ac.uk

Summary

The Clarion Clipperton Zone (CCZ) is the focal region for imminent deep-sea nodule mining[1], yet fundamental questions remain about ecosystem resilience[2]. To protect the marine environment in the CCZ, the International Seabed Authority (ISA) designated Areas of Particular Environmental Interest (APEIs)[2,4]. Connectivity was not a formal criterion in the original APEI design[5,6], but has since gained prominence in ISA policy[7]. Use larval dispersal modelling and network analysis, we assess the connectivity of the APEI design. APEIs show internal cohesion and provide some larval input to areas of mining interest (AMIs), especially after 2021 additions[4]. However, the 'network' of APEIs is not functioning: APEIs are largely disconnected: fewer than 0.02% of simulated larvae disperse between protected areas, and most are functioning as isolated units. This weak connectivity limits the network's effectiveness in a biologically variable region and undermines its capacity to sustain populations or support recovery following mining disturbance[2]. Most larval replenishment to AMIs originates outside both APEIs and AMIs, revealing opportunities to enhance APEI support for ecosystem resilience. Strategic expansion, totalling a 47% increase in protected area, could lead to full APEI connectivity, increasing inter-APEI connectivity 406-fold and nearly doubling larval input to AMIs[8,9], strengthening conservation outcomes prior to mining.

Introduction

The deep ocean is rapidly becoming the next frontier for commercial mineral extraction. At the heart of this is the Clarion Clipperton Zone (CCZ), a 6 million km^2 swathe of the central Pacific seabed of interest for mining polymetallic nodules - a type of rock rich in minerals critical to modern technologies[1]. With over a million square kilometres already under licence for exploration[10], the developments for mining the deep sea are accelerating, outpacing our understanding of its ecosystems[11,12]. The CCZ is not only species-rich, but also ecologically complex[13], and managing its biodiversity in the face of industrial disturbance remains a formidable challenge[2].

To help manage the potential effects of mining, the International Seabed Authority (ISA)[3] established a network of protected areas known as Areas of Particular Environmental Interest (APEIs). These were designed to represent diverse habitats and buffer mining impacts, but connectivity was not a formal criterion[5,6]. A further expansion in 2021 brought the total protected area to nearly two million square kilometres[4], with an increased prominence of connectivity in ISA policy[7]. Connectivity is important, because a key component of an effective and self-sustaining network of MPAs/APEIs is coherence [9,14], however, the spatial arrangement of the APEIs and thus capacity to function as a coherent ecological network remains untested.

Connectivity is critical to marine spatial planning[15], central to conservation targets[16] and important in maintaining ecological attributes[17], such as biodiversity[18]. In the deep sea, many species depend on larval dispersal to link fragmented populations[19]. Ocean currents carry larvae between habitats, enabling recolonisation and preserving genetic diversity[20,21]. Without sufficient connectivity, isolated populations may fail to recover from disturbance - a key concern for mining scenarios.

Here, we apply larval dispersal modelling and network analysis to provide evidence-based management approaches to address a critical emerging threat to largely pristine abyssal systems. To address data scarcity typical of these environments which has hampered connectivity-relevant APEI design and analysis in the past[5], we use an "everything is everywhere" approach (*sensu* James et al. 2024)[22]: assuming uniform larval release potential across the seafloor to reveal all plausible dispersal pathways. This enables the identification of potential sources, sinks, and corridors across both protected and unprotected areas. We assess the coherence of the current APEI network, characterise the structure of larval dispersal across the CCZ, evaluate the potential for APEIs to replenish areas of mining interest (AMIs - including both current ISA exploration contracts and reserved areas), and identify currently unprotected regions critical to maintaining ecological connectivity. Our approach provides a generalisable framework for data-limited conservation planning in frontier regions like the deep ocean.

Results

APEIs support internal cohesion but do not function as a connected network

Our results found that APEIs in the CCZ exhibit near-total isolation (Figure 1). Across all simulations, just 0.018% of particles dispersed between APEIs, whilst 78.56% remained within their origin, and 21.42% settled outside the network entirely. Of 156 possible direct APEI-to-APEI connections, only five showed any exchange - dominated by three routes: APEI 5 to 8, APEI 8 to 9, and APEI 13 to 9, which together accounted for over 99% of all transfers. The only other direct links, APEI 2 to 13 and APEI 6 to 3, involved fewer than 15 particles each. Two additional pathways showed potential for indirect connectivity, via sequential settlement through intermediate APEIs: APEI 2 to APEI 9 via APEI 13, and APEI 5 to APEI 9 via APEI 8.

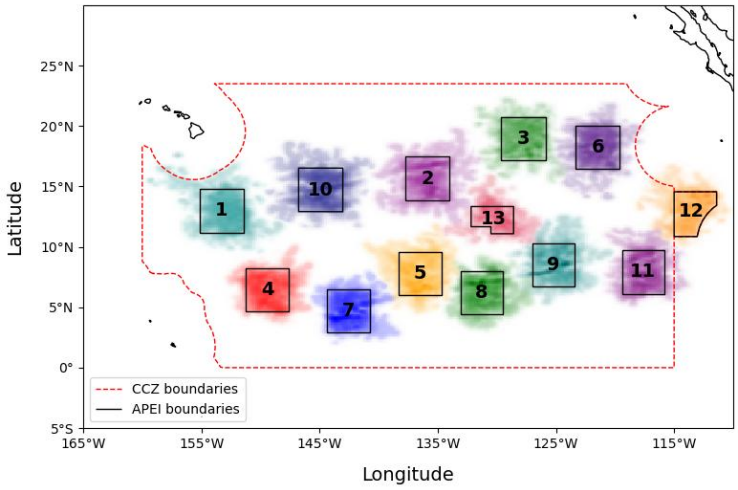


Figure 1: Larval dispersal footprints and spatial configuration of the 13 APEIs (outlined in black) in the Clarion Clipperton Zone, numbered according to their official designation. Coloured dispersal footprints represent the spatial extent of larval settlement originating from each APEI at the end of their planktonic larval duration (PLD) (cumulative results for 19-,35- and 69 days of simulated dispersal for 4 time periods: January 2019; July 2019; January 2023; and July 2023), overlaid on the CCZ management region (red dashed boundary).

Self-retention of particles within the APEI from which they originated was consistently high. APEIs 3 and 6 retained 87.7% and 85.5% of their particles, respectively, while APEI 13 - the least retentive - retained 60.4%. Even under maximum simulated dispersal (69 days[19]), median travel distances remained under 100 km (Ext. Dat. Fig 1) - far below the 200–800 km gaps between APEIs[23]. For particles that failed to settle in an APEI, the median distance to the nearest non-origin APEI was still large at 388.7 km (IQR: 297.9–542.3 km), indicating that also multi-generational functional connectivity may be limited, even assuming the transitional areas remain suitable for successful reproduction, which may not be the case if mining occurs in such transitional areas.

APEIs can support nearby areas of mining interest

While direct connectivity between APEIs is limited, they do supply larvae to other parts of the CCZ, including designated areas of mining interest (AMIs). After 69 days of dispersal, an upper estimate of planktonic larval duration[19], 86% of designated AMI sites had received particles from APEIs. Testing shorter PLDs of 35 and 19 days, connectivity to AMIs was reduced to 66% and 44% of AMIs, respectively, highlighting the importance of dispersal duration. Overall, only 4.6% of particles released from APEIs reached AMIs. Contribution varied considerably across individual APEIs. APEI 13 was the strongest contributor to AMIs, accounting for over 21% of APEI-derived settlement. APEI 2 also contributed well, supplying nearly 18% of larvae reaching AMIs. In contrast, APEIs 6, 7, and 10 showed minimal contribution to AMIs and APEI 8 had none.

Most larval input to AMIs comes from outside the protected network. Several unprotected areas also not designated for mining activity - often adjacent to APEIs - emerged as dominant sources of larval supply (Figure 2). These areas consistently outperformed APEIs in both particle density and spatial reach. Their contributions were not only greater in volume but also more widespread, delivering larvae to multiple potential mining regions across the CCZ.

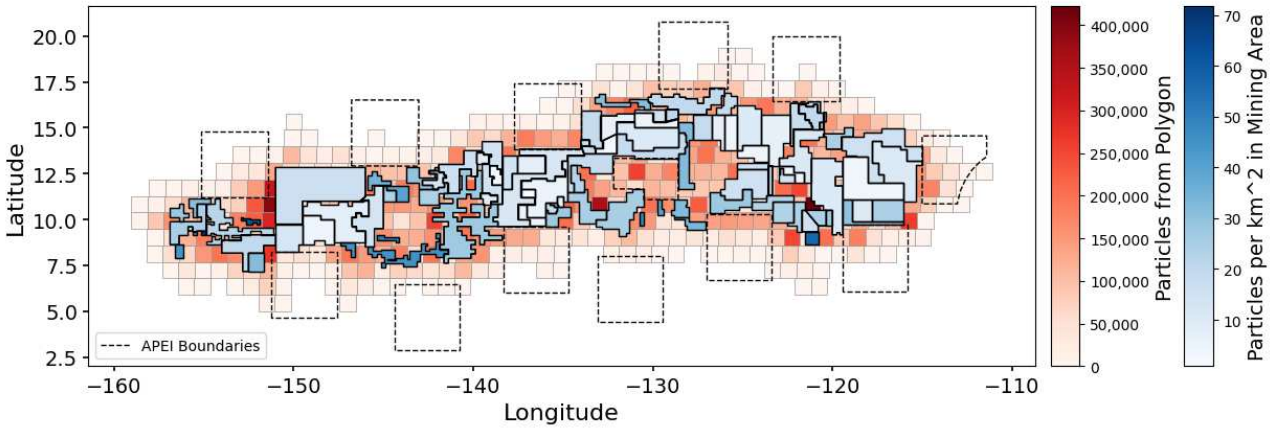


Figure 2: Origin density (red) and settlement density (blue) of larval particles that settle in areas of mining interest (AMIs), released from all cells outside the AMIs (including both APEIs and unprotected, non-mining areas). Mining areas (exploration and reserved zones combined) are shown as blue polygons. Darker blue shades indicate higher settlement densities, representing greater larval influx into mining areas. Red shading shows the density of particles originating from source cells that contributed larvae to mining areas.

These findings highlight a critical gap: the current APEI network contributes little to potential mining zone replenishment, while key larval sources remain unprotected. While it could be argued that these

areas are de facto protected due to their location outside exploration contract areas, this does not guarantee long-term legal protection. Simply being outside of current contract zones doesn't provide assurance that these areas will remain free from future exploitation or disturbance without an official protected status.

Connectivity in the CCZ is modular, local, and vulnerable to mining losses

Larval dispersal in the CCZ is strongly modular, with movement largely confined within four major connectivity communities (Figure 3).

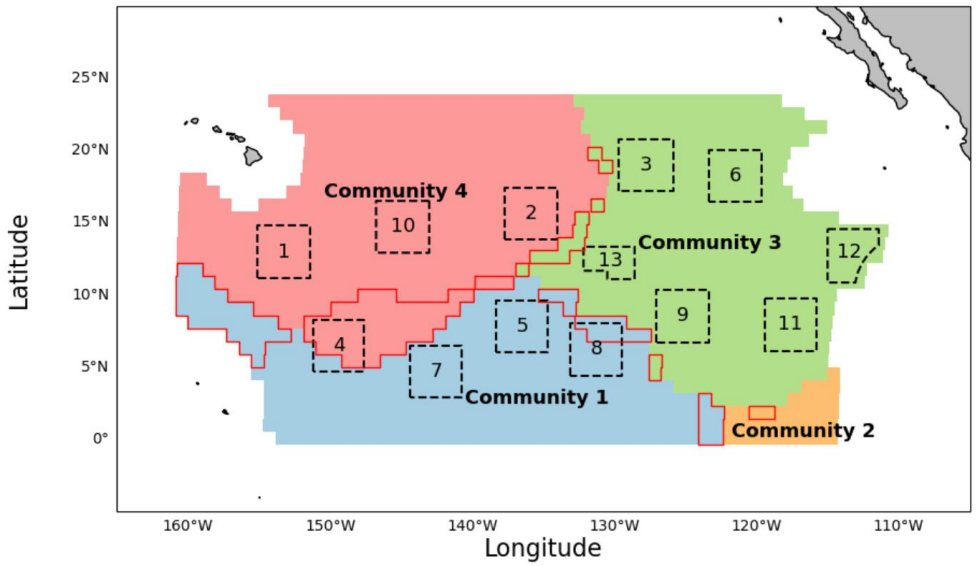


Figure 3: Community structure of larval connectivity in the Clarion Clipperton Zone showing four distinct larval connectivity communities across the CCZ, derived from simulated dispersal trajectories. Coloured areas represent community membership, while dashed black squares indicate the locations of APEIs. Interface zones outlined in red shift community affiliation when mining-origin larvae are removed.

Community 4, in the northwest, is the largest and best connected, spanning 4.41 million km² (36% of the CCZ), while Communities 1 and 3 together cover over 60% of the region. Despite being the smallest, Community 2 displayed the highest internal connectivity, but contains no APEIs, revealing a critical gap in protection.

Under current conditions, connectivity between communities is limited, with the majority of larval exchange occurring within rather than across community boundaries (Extended Data Fig. 2, left panel). When larvae originating from mining areas are excluded, representing a plausible mining scenario, connectivity declines across the network (right panel), with both intra- and inter-community flows reduced. Community 4 experiences particularly large losses, with a 23% reduction in outward dispersal and 24% decline in larval input. Several regions (outlined in red in Fig. 3) shift their community assignment under this scenario, highlighting their sensitivity to changes in larval supply. These areas sit at the boundaries of community partitions and appear to be structurally flexible, changing affiliation depending on larval sources. This suggests they are influenced by multiple connectivity pathways and may contribute to maintaining links between otherwise distinct communities. In a mining scenario, their sensitivity and positioning make them vulnerable to disruption, but also potentially important for preserving residual connectivity. Protecting these

regions could therefore help buffer against fragmentation and support the adaptive capacity of the system in the face of environmental change.

Critical connectivity zones remain unprotected

Grid cells that maintain high connectivity value even under potential mining-induced source loss occur around the AMIs (Figure 4).

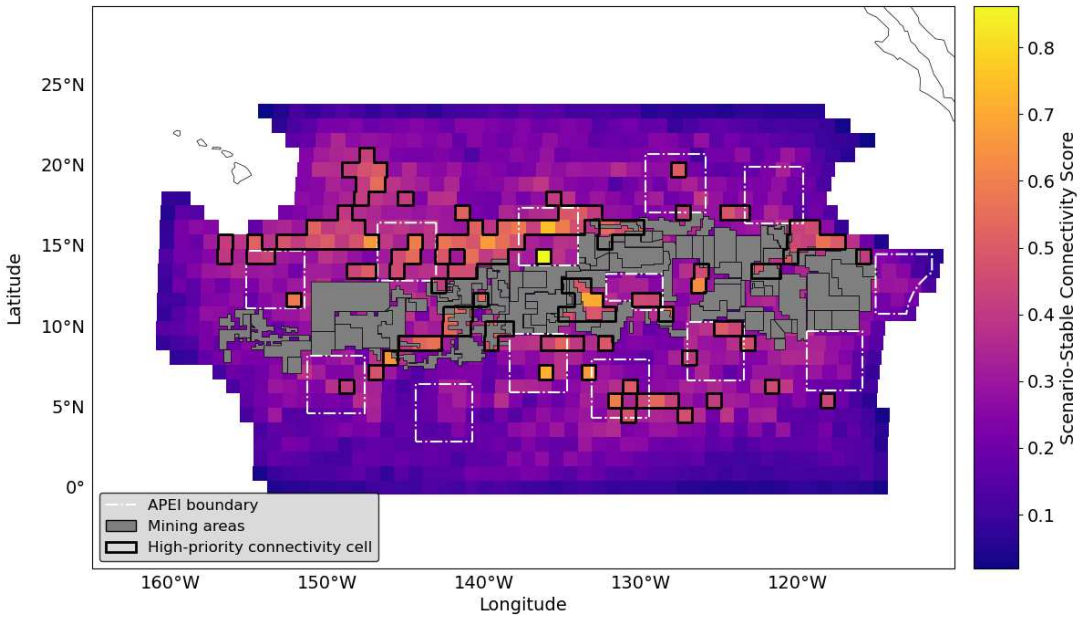


Figure 4: Scenario-stable composite connectivity score for 100×100 km grid cells across the CCZ, integrating source strength (out-degree) and stepping-stone potential (node betweenness) under both non-mining and post-mining scenarios (*see Methods*). Black-outlined cells represent the top 10% of scenario-stable scores. AMIs are shown in grey and APEI boundaries in dashed white. Scores reflect each cell's ability to support connectivity across conditions; warmer colours indicate higher, more persistent connectivity.

The cells outlined in black represent the top 10% of locations that consistently function as larval sources and stepping stones for connectivity throughout the CCZ (not just to AMIs) in both mining and non-mining scenarios, where in the 'mining' scenario the AMIs no longer function as larval sources due to mining activities. Spatially, these high-priority cells are widely distributed, with 77% of their total area falling outside existing APEIs, and many occur along margins of AMIs, underscoring critical gaps in current spatial coverage. Their persistence across mining and non-mining scenarios suggests they are robust features of the CCZ dispersal landscape and thus prime candidates for targeted conservation action.

Extending the network: The strategic placement of new protected areas

To test whether the network's shortcomings could be addressed, we developed a spatial prioritisation framework to identify the minimum set of new sites needed to restore connectivity. The resulting configuration transformed network performance (Figure 5). While direct APEI-to-APEI links remained unchanged, the inclusion of new protected sites would enable 151 indirect pathways, increasing inter-APEI dispersal 406-fold (40500%) - from just 1 in 5,556 particles to 1 in 14 released from protected areas reaching another protected area. The new sites act as corridors between current APEIs and become key stepping stones, capturing 20.9% of particles from current APEIs and

returning 8.1% back into the network, while halving the median near-miss distance of unsuccessful dispersers from 388.7 km to 153.8 km. Addition of the corridors also improves connectivity to AMIs: contributions increased from 4.6% to 7.8%, representing a 69% increase in supply driven predominantly by 3 new sites: (Figure 5: inset; dark, brown, light brown, green)). The proportion of AMIs receiving larvae rose from 86.2% to 95.0%, with gains across all larval dispersal durations.

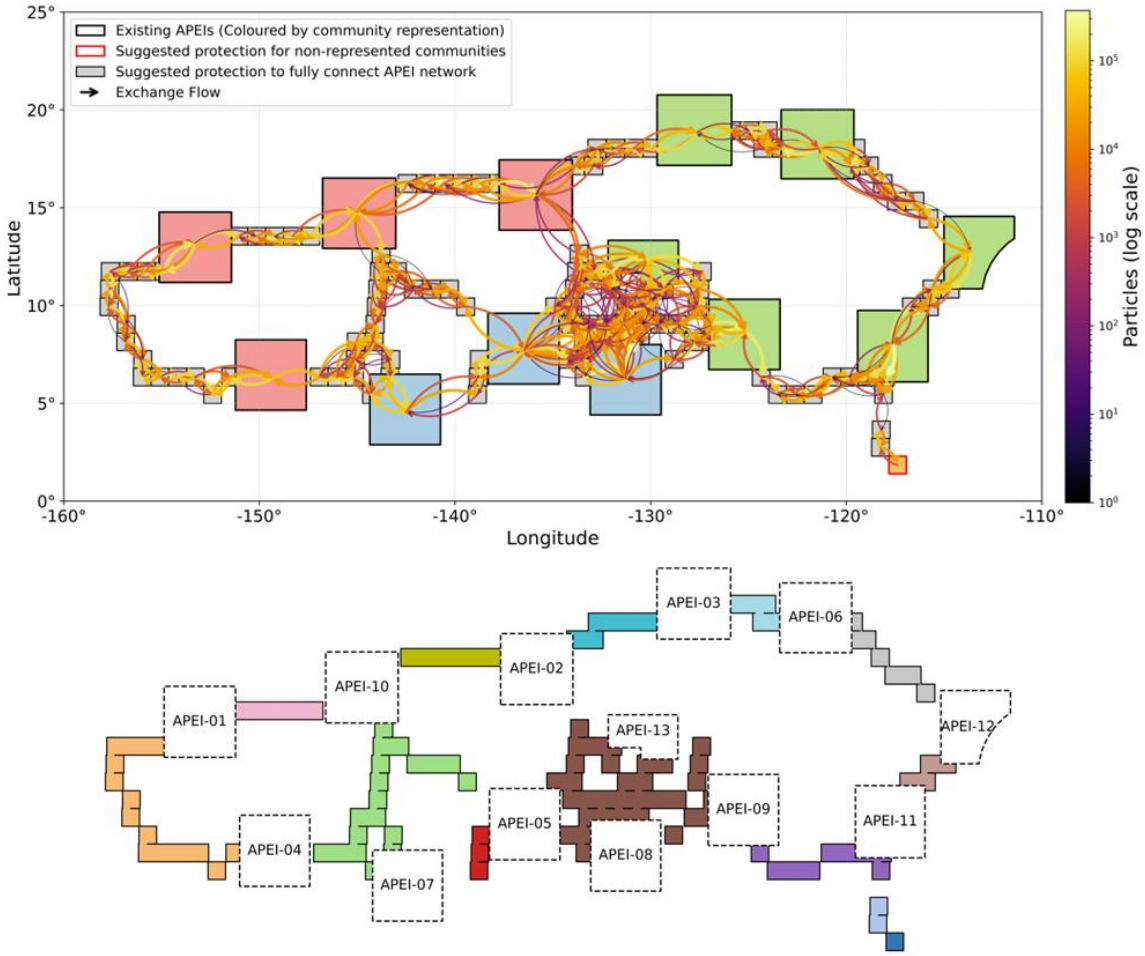


Figure 5: *Top:* Enhanced APEI network with particle exchange flows showing the optimised protected area configuration, including existing APEIs (coloured by community), and suggested additions to connect the network (black outline), and represent previously unprotected communities (red outline: one box). Arrows indicate larval exchange flows between sites, with colour intensity scaled by particle count ($\log_{10}$). *Bottom*: shows the grouped configuration of the 13 sites proposed to enhance APEI connectivity.

Discussion

Our analysis provides the first region-wide predictive assessment of ecological connectivity in the Clarion Clipperton Zone (CCZ) and reveals potential for improvement in the current APEI network. Although modified in 2021 to improve habitat representation[24], the network still falls short of functioning as a coherent ecological system. Connectivity between APEIs is virtually absent. This isolation may limit the ability of the APEI network in supporting biodiversity at regional scales[3,4]. Despite their fragmentation, APEIs can supply larvae to nearby areas of mining interest (AMIs), suggesting potential for localised recovery, but these contributions are limited. More broadly, dispersal across the CCZ is structured into four semi-isolated connectivity communities, many of which depend on key regions that currently fall entirely outside the protected network. These unprotected nodes play a disproportionate role in maintaining exchange within and between communities.

Without intervention, mining-driven source loss will erode these important links, severing large portions of the CCZ from regional dispersal pathways and weakening the system's capacity for natural recovery. Preserving these ecological corridors is suggested in future management strategies.

A network only by name

The APEI system was designed on the assumption that 200 × 200 km reserves (with 100 km buffers), spaced 400–800 km apart, would allow for both self-recruitment and larval exchange[23,25]. Although the original and extended networks were designed based on environmental representation[6,24], the importance of connectivity between APEIs was formally acknowledged during the 2019 Friday Harbor workshop, which highlighted genetic connectivity as a key consideration in the region's environmental management but recognising extreme data scarcity[26]. However, our simulations show that realised larval dispersal distances are far too small to span the current distances between APEIs[27], resulting in high self-retention and extremely little inter-APEI exchange. This aligns with prior findings that actual dispersal is often much shorter than theoretical expectations[28,29,30], and exposes a weakness in the design: while the network represents biodiversity[24] and supports largely self-sustaining regions through high levels of self-recruitment, it fails to establish functional connectivity standards essential for ecological resilience[8,9,31].

The solution does not require a complete overhaul of the network. Many dispersal distances narrowly miss their targets, revealing opportunities to enhance connectivity by strategically adding bridging corridors within range. These latent connections, once activated, can transform an isolated set of reserves into a functionally coherent network. Achieving this requires moving beyond static design templates toward adaptive, evidence-based spatial planning.

Performance disparities among APEIs also challenge the idea that all nodes contribute equally. Sites with low connectivity are not expendable - they capture unique habitats[24] - but their limited role in system-wide recovery highlights the need for complementary strategies.

Unprotected, indispensable: The role of non-protected areas

Several of the most strategically important areas for sustaining ecological connectivity in the CCZ lie entirely outside the existing network of protected zones. These sites consistently function as larval sources and critical stepping-stones, enabling movement between otherwise isolated regions even under scenarios where larvae are lost to mining activity. Their structural importance and persistence across undisturbed and disturbed scenarios highlight them as essential, long-term contributors to regional resilience.

Many of these high-performing cells are located closer to mining zones than to any APEI. Given the limited dispersal distances observed, this spatial alignment is not incidental - it is pivotal. These areas are not passive conduits but active nodes that uphold network cohesion and facilitate ecological recovery. Prioritising their conservation, particularly those that serve dual roles as exporters and connectors, would substantially strengthen the functional integrity of the CCZ[32]. Moreover, where such areas overlap with habitat types targeted for extraction, they could serve as valuable preservation reference zones[33] or potentially inform relinquishment decisions[34.]

Partitioned by nature, neglected by design: Unequal protection of semi-isolated communities

The CCZ is not a single connected system, but a patchwork of semi-isolated larval dispersal communities. Our analysis revealed four distinct connectivity regions, within which larval movement is largely retained. These patterns mirror emerging biogeographic structure across the CCZ[35] and are

supported by genetic evidence of population subdivision in species like the sponge *Plenaster craigi* pointing to limited dispersal across regional boundaries[36].

The current APEI network fails to reflect this natural partitioning. One entire connectivity community (Community 2) remains completely unprotected, despite exhibiting the highest internal connectivity density and smallest spatial footprint, thus giving it heightened vulnerability to localised disturbance[37]. Meanwhile, other communities depend on a small number of unprotected bridging zones to maintain inter-regional exchange. These links are ecologically fragile: when mining-source larvae are removed, connectivity between communities collapses, leaving large areas isolated and unable to recover.

This misalignment exposes a critical vulnerability. Resilience depends not only on protecting representative habitat, but on anchoring each connectivity community with functionally active nodes. Without this, larval replenishment after disturbance will be confined within fragmented compartments, undermining regional recovery and deviating from core principles of ecosystem-based management. A connected network should not exclude entire communities.

Mind the Gaps: Redesigning Protection for Deep-Sea Connectivity

Connectivity is not an abstract concept but a measurable, implementable design feature. Both IUCN[8] and OSPAR[9,31] stress that networks must be large, connected, and representative to sustain populations and ecological processes, including larval sources and refugia[38], and should be based on the best available science[31] and the precautionary principle[8,9]. Our approach puts this into practice by prioritising dynamic processes over static boundaries. By integrating connectivity science into reserve design - using a new Integrated Connectivity Value (ICV) and dispersal-informed optimisation to identify the shortest biologically relevant paths between disconnected APEIs - we identified a minimal set of additions that transform network performance, balancing ecological function with spatial efficiency, and offering a scalable blueprint for adaptive conservation in dynamic, data-poor systems[39-41]. As new Regional Environmental Management Plans (REMPs) including networks of protected areas are developed by the ISA for regions like the Mid-Atlantic Ridge and Indian Ocean, our findings demonstrate that integrating larval connectivity into design is both feasible and essential, shifting protection from static coverage to process-based resilience and transforming the regions from fragmented patchwork into connected systems.

Conclusion

We show that connectivity can be mapped, measured, and integrated into marine spatial planning, even under conditions of ecological uncertainty. We strongly recommend adopting the practice to embed connectivity into conservation design, adapt it as data improves, and act before irreversible damage occurs. Optimising the APEI network based on connectivity offers a chance to move from fragmented protection toward a resilient, future-ready framework. An updated network, grounded in multidisciplinary data - from ocean modelling to connectivity science to emerging biological insights - can deliver smarter, more resilient protection.

References

1. Hein, J. R., Koschinsky, A. & Kuhn, T. Deep-ocean polymetallic nodules as a resource for critical materials. *Nat. Rev. Earth Environ.* **1**, 158–169 (2020).
2. Levin, L. A. *et al.* Defining "serious harm" to the marine environment in the context of deep-seabed mining. *Mar. Policy* **74**, 245–259 (2016).
3. International Seabed Authority. Decision of the Council relating to an environmental management plan for the Clarion-Clipperton Zone. ISBA18/C/22. (2012).
4. International Seabed Authority. Decision of the Council relating to the review of the environmental management plan for the Clarion-Clipperton Zone. ISBA26/C/58. (2021).
5. International Seabed Authority. Environmental management plan for the Clarion-Clipperton Zone (ISBA/17/LTC/7). (2011)
6. Wedding, L.M. *et al.* From principles to practice: a spatial approach to systematic conservation planning in the deep sea. *Proc. Roy. Soc. B: Biol. Sci*, **280** (1773), 20131684.
7. International Seabed Authority. Review of the environmental management plan for the Clarion-Clipperton Zone (ISBA/26/C/43). (2021)
8. IUCN. *Global Standard for Nature-based Solutions: A user-friendly framework for the verification, design and scaling up of NbS.* 1st edn . IUCN, Gland. (2020).
9. OSPAR Commission. *Guidance on developing an ecologically coherent network of OSPAR*
10. International Seabed Authority. Consolidated Regulations on Prospecting and Exploration for Polymetallic Nodules in the Area. ISBA/19/C/17. (2013).
11. Simon-Lledó, E. *et al.* Megafaunal variation in the abyssal landscape of the Clarion Clipperton Zone. *Prog. Oceanogr.* **170**, 119–133 (2019).
12. Smith, C. R., Clark, M. R., Goetze, E., Glover, A. G. & Howell, K. L. Editorial: Biodiversity, connectivity and ecosystem function across the Clarion-Clipperton Zone: A regional synthesis for an area targeted for nodule mining. *Front. Mar. Sci.* **8**, 797516 (2021).
13. Simon-Lledó, E. *et al.* Carbonate compensation depth drives abyssal biogeography in the northeast Pacific. *Nat. Ecol. & Evol.*, *7* (9), 1388-1397 (2023).
14. Gardner, J.P., Lausche, B., Pittman, S.J. & Metaxas, A. Marine connectivity conservation: Guidance for MPA and MPA network design and management. *Mar. Pol.*, ***167***, 106250 (2024).
15. Virtanen, E. A., Moilanen, A. & Viitasalo, M. Marine connectivity in spatial conservation planning: analogues from the terrestrial realm. *Landsc. Ecol.* **35**, 1021–1034 (2020).
16. Keeley, A.T., Beier, P. & Jenness, J.S. Connectivity metrics for conservation planning and monitoring. *Bio. Con.*, *255*, 109008. (2021)
17. Preston, J. *et al.* Seascape connectivity: evidence, knowledge gaps and implications for temperate coastal ecosystem restoration practice and policy. *npj Oce. Sus.*, *4*(1), 33. (2025)
18. Fontoura, L. *et al.* Protecting connectivity promotes successful biodiversity and fisheries conservation. *Sci*, *375*(6578), 336-340 (2022).
19. Hilário, A. *et al.* Estimating dispersal distance in the deep sea: challenges and applications to marine reserves. *Front. Mar. Sci.* **2**, 6 (2015).
20. Selkoe, K. A. *et al.* A decade of seascape genetics: contributions to basic and applied marine connectivity. *Mar. Ecol. Prog. Ser.* **554**, 1–19 (2016).
21. Young, C. M. Reproduction, development and life-history traits. In *Ecosystems of the Deep Oceans* (ed. Tyler, P. A.) 381–426. Elsevier, Amsterdam. (2003).

22. James, M. K. *et al.* The 'everything is everywhere' framework: Holistic network analysis as a marine spatial management tool. *Ecol. Inform.* **80**, 103105 (2025).
23. Smith, C. R. *et al*. Rationale and recommendations for the establishment of preservation reference areas for nodule mining in the Clarion-Clipperton Zone. *Legal and Technical Commission, International Seabed Authority, Technical document no. ISBA/14/LTC/2* (2008).
24. McQuaid, K.A. *et al.* Using habitat classification to assess representativity of a protected area network in a large, data-poor area targeted for deep-sea mining. *Front. Mar. Sci.*, 7, 558860 (2020)
25. Botsford, L. W., Hastings, A. & Gaines, S. D**.** Dependence of sustainability on the configuration of marine reserves and larval dispersal distance. *Ecol. Lett.* **4**, 144–150 (2001).
26. International Seabed Authority. Deep CCZ Biodiversity Synthesis Workshop, Friday Harbor Laboratories, Washington. (2019).
27. Kinlan, B. P. & Gaines, S. D**.** Propagule dispersal in marine and terrestrial environments: a community perspective. *Ecology* **84**, 2007–2020 (2003).
28. Shanks, A. L. Pelagic larval duration and dispersal distance revisited. *Biol. Bull.* **216**, 373–385 (2009).
29. James, M. K., Polton, J. A., Mayorga-Adame, C. G., Howell, K. L. & Knights, A. M. Assessing the influence of behavioural parameterisation on the dispersal of larvae in marine systems. *Ecol. Model.* **476**, 110252 (2023).
30. Firth, L. B. *et al.* Ocean sprawl: challenges and opportunities for biodiversity management in a changing world. *Oceanogr. Mar. Biol. Annu. Rev.* **54**, 189–262 (2016).
31. OSPAR Commission. *Marine Protected Areas*. Reference no. 2006-3. London (2006)
32. Wedding, L. M. *et al.* Managing mining of the deep seabed. *Science* **349**, 144–145 (2015).
33. International Seabed Authority. Workshop on the design of Impact Reference Zones and Preservation Reference Zones in the Area, Berlin, Germany. (2017).
34. International Seabed Authority. Decision of the Council of the International Seabed Authority relating to amendments to the Regulations on Prospecting and Exploration for Polymetallic Nodules in the Area and related matters. ISBA/19/C/17 (2013).
35. Simon-Lledó, E. et al. Marked variability in distance-decay patterns suggests contrasting dispersal ability in abyssal taxa. *Glob. Ecol. Biogeogr.* **34**, e13956 (2025).
36. Taboada, S. et al. Implications of population connectivity studies for the design of marine protected areas in the deep sea: an example of a demosponge from the Clarion-Clipperton Zone. *Mol. Ecol.* **27**, 4657–4679 (2018).
37. Boschen, R.E., Rowden, A.A., Clark, M.R., Pallentin, A. & Gardner, J.P. Seafloor massive sulfide deposits support unique megafaunal assemblages: implications for seabed mining and conservation. *Mar. env. Res.* **115**, 78-88. (2016).
38. Chape, S., Blyth, S., Fish, L., Fox, P. & Spalding, M. 2003 United Nations List of Protected Areas. IUCN & UNEP-WCMC, Gland, Switzerland and Cambridge, UK. (2003).
39. Game, E.T., Watts, M.E., Wooldridge, S. & Possingham, H.P. Planning for persistence in marine reserves: a question of catastrophic importance. *Ecol. App.*, **18**(3), 670-680. (2018).
40. Wilson, K.A., Carwardine, J.& Possingham, H.P. (2009) Setting conservation priorities. *Annals of the New York Academy of Sciences*, *1162*(1), pp.237-264.
41. Grorud-Colvert, K. *et al.* Marine protected area networks: assessing whether the whole is greater than the sum of its parts. *PloS one*, *9*(8), p.e102298. (2014).

Data Availability

Data and code can be made available upon request

Acknowledgements

This study is part of the Seabed Mining And Resilience To EXperimental impact (SMARTEX) project funded by the UK's Natural Environment Research Council (NERC) grant number NE/T00293X/2.

This work used the ARCHER2 UK National Supercomputing Service (https://www.archer2.ac.uk).

Author Contributions

MKJ: Conceptualization; Methodology; Software; Validation; Formal Analysis; Investigation; Data Curation; Visualisation; Writing-Original Draft. AEHB: Conceptualization; Methodology, Writing – Review & Editing. DOBJ: Conceptualization, Writing – Review & Editing, Project Administration, Funding Acquisition. AMK: Conceptualization; Methodology; Writing – Review & Editing. CHC: Software; Resources; Writing – Review & Editing. DdJ: Writing – Review & Editing. KLH: Conceptualization; Writing – Review & Editing, Project Administration, Funding Acquisition.

Competing Interests

The authors declare no competing interests

Methods

The study area

A uniform 100 × 100 km (10,000 km²) grid was generated across the CCZ region (160°-110°W, 0°-25°N), balancing spatial resolution with computational efficiency for connectivity analysis. To account for Earth's curvature, latitude and longitude offsets were adjusted per cell size. Land polygons from Natural Earth[42] were used via the 'cartopy' package[43] to exclude terrestrial cells. The grid was clipped to the CCZ management area[44], resulting in 1,225 ocean-only cells (Ext. Dat. Fig. 3).

The biophysical model

The hydrodynamic model

The GOFS 3.1 HYCOM model[45] provides 41-layer global ocean circulation data at 0.08 × 0.04° horizontal resolution (~9 × 4.5 km). Zonal ('water_u_bottom') and meridional ('water_v_bottom') bottom-layer velocities were retrieved at 3-hour intervals for 170-110°W, 5°S-25°N, spanning January 2019-September 2023. Spatial bounds extended 10° latitude and 5° longitude beyond the CCZ to capture full particle trajectories within their planktonic larval durations. Bottom velocities represent flow 10 m above the seafloor and follow GEBCO-derived bathymetry[46].

Several limitations apply to HYCOM's use in deep-sea settings. Observational data for model validation at the seafloor are sparse, especially in remote Pacific regions. Bottom boundary layer processes are parameterised[47] but may miss near-bed turbulence and fine-scale dynamics. Resolution limits topographic steering and fails to resolve small bathymetric features. Episodic events like eddy-driven current reversals[48] are also not captured. These factors may lead to overestimated connectivity

between communities and underestimated local retention, while obscuring rare but ecologically important long-distance dispersal. While these factors do not invalidate the model's use for broadscale interpretation, they should be considered when evaluating fine-scale or event-driven seafloor connectivity patterns.

Lagrangian particle tracker

Particle tracking was performed using Ocean Parcels v2.1[49], forced by the hydrodynamic model. Simulations were run for January and July in both 2019 and 2023 to capture inter- and intra-annual variability, including El Niño/La Niña phases[50,51,52,53] (Ext. Data Tab. 1). Particles were released every 25 km across the CCZ[22], yielding 18,679 unique release sites (~16 per 100 × 100 km cell). Trajectories were simulated for up to 69 days, the upper quartile of deep-sea planktonic larval durations[19], using a 2D fourth-order Runge–Kutta advection scheme with stochastic diffusion (see *Diffusivity*). To minimise behavioural uncertainty, particles were constrained to the bottom layer (10 m above the seafloor) - a conservative approach based on the assumption that many abyssal species, especially weak swimmers, remain near the seabed during dispersal. This seabed-following method reflects the limited understanding of deep-sea larval behaviour, as incorrect parameterisation (e.g. vertical swimming) can significantly distort dispersal predictions[54,55]. Dispersal distances were estimated as great-circle distances between release and settlement points using the haversine formula, accounting for Earth's curvature[56]. While not reflecting exact trajectories, this provides a reliable measure of dispersal extent for assessing deep-sea connectivity patterns.

Diffusivity

To simulate sub-grid scale horizontal movement, we implemented a stochastic diffusion scheme using the Smagorinsky method[57] within Ocean Parcels. Horizontal eddy diffusivity was calculated from local velocity gradients using a Smagorinsky constant (Cs = 0.1) and a central difference approach with a spatial offset (dx = 0.01°). Velocity components (U, V) were extracted at ±dx in both longitude and latitude to compute gradients: *dudx, dudy, dvdx*, and *dvdy*. These were used alongside the area of the computational cells (A) to calculate horizontal diffusivity (Kh) as:

$$Kh = Cs \times A\sqrt{dudx^2 + 0.5 \times (dudy + dvdx)^2 + dvdy^2}\ .$$

Stochastic displacement was drawn from a normal distribution based on Kh and the model timestep (random walk)[58], simulating variability from turbulent flow, and added to the particles position. A fixed random seed ensured reproducibility, isolating hydrodynamic differences between simulations from random variation.

Sensitivity analysis

Several tests were undertaken to identify the optimal internal model timestep and optimal number of particles released from each site for accurate representation and computational feasibility

Internal timestep

To ensure numerical stability and accuracy, we applied the Courant-Friedrichs-Lewy (CFL) condition[59] which requires that particles travel less than one grid cell per timestep. This is expressed as:

$$CFL = \frac{U \times \Delta t}{\Delta x} \leq C_{max}$$

Where U is the maximum current velocity (in m/s), Δt is the hydrodynamic model timestep (in seconds), Δx is the spatial resolution of the model grid (in meters) and C_{max} is 1 for model stability. At the hydrodynamic model's native 3-hour timestep and resolution, the CFL number was 0.509 - within stable limits. However, as it is suggested to use an internal timestep that is less than the temporal resolution of the underlying model in particle tracking studies to capture the dynamics of larval interactions with hydrodynamic features[60,61] , we adopted a 1-hour internal timestep, reducing the CFL to 0.2 and improving model fidelity.

Optimal particle number

To determine an optimal number of particles per release site (PPS), we ran simulations for 69 days with PPS values ranging from 100 to 10,000. For each run, we recorded particle start and end cell IDs and calculated the number of unique cell-to-cell connections. We then fitted a logarithmic model using SciPy's 'curve fit' function[62] to describe the relationship between PPS and the number of unique connections, capturing the pattern of diminishing returns (Ext. Data Fig. 4). To quantify this effect, marginal return was calculated as the change in unique connections per 100 additional particles per site. This approach aligns conceptually with Simons et al.[63], who used variance-based thresholds, but here a curve-fitting method was used to suit scalar connectivity data and improve computational efficiency. The point of diminishing returns was defined as a marginal gain of fewer than 1 unique connection per additional 100PPS, reached at ~400 PPS. A "flatline" point - where gains fell below 0.1 unique connections per additional 100PPS - was identified at ~3,600 PPS. To ensure compatibility with parallel processing, this was rounded up to 3,648 PPS, yielding 68,140,992 particles per simulation across all 1,225 release sites.

Accounting for variation

To capture seasonal and interannual variability, we ran simulations for four time points (Ext. Dat. Tab. 2), with particle positions recorded at 19, 35, and 69 days - representing the median and interquartile ranges of deep-sea planktonic larval durations[19]. We then calculated Jaccard dissimilarity[64] for each pairwise comparison (e.g., Jan 2019 vs. July 2019) to assess differences in dispersal pathways, based on binary representations of cell-to-cell connections, and used Cohen's Kappa[65] to quantify similarity in connectivity patterns. To test whether observed Jaccard values exceeded random expectation, we performed a permutation test by shuffling one array 9,999 times to generate a null distribution (Ext. Data Tab. 3). Simulations showing statistically distinct connectivity patterns were combined prior to connectivity analysis to provide an integrated view of connectivity across seasonal and interannual scales.

Connectivity Assessments

To assess both the interconnectedness of the existing APEI network and the broader-scale connectivity patterns across the CCZ, the particle tracking simulation outputs were used to perform a number of analyses.

APEI Network Functionality

We first isolated particles released from within APEIs, allowing assessment of retention and exchange within the designated protected areas. To generate summary connectivity metrics, Particles were tracked from release to settlement, and counts were aggregated by source and destination APEI. For those settling outside the APEI network, we identified the nearest APEI and calculated settlement distance, enabling detection of "near misses" - instances where larvae settled just beyond protection

boundaries. This analysis quantified per-APEI retention, pairwise exchange, and dispersal proximity, revealing the strengths and spatial gaps in the APEI network.

To evaluate the role of APEIs in supporting impacted regions, we further identified particles released from APEIs that settled within mining contract areas. This allowed us to calculate the proportion of mining zones receiving larvae from APEIs, assess which APEIs contributed most to mining-area recruitment, and determine what share of APEI-released particles ultimately reached these vulnerable zones. It is important to note that we did not evaluate the habitat suitability of potential source areas and assumed equal suitability across the network.

APEI support score

1. To quantify each polygon's contribution to APEI connectivity, we defined an *APEI support score* that integrates both the volume and diversity of larval exchange. This metric reinforces internal connectivity and reflects whether protected populations can support one another through natural dispersal, promoting long-term persistence. It is based on realised larval dispersal rather than geometric proximity[66].

The score is calculated as:

$$A_i = (S + R) \cdot \left(1 + 2 \cdot \frac{\min(S, R)}{S + R}\right) \cdot (N_s + N_r)$$

where S and R are the number of particles sent to and received from APEIs, and N_s, N_r are the number of distinct APEIs to which particles were sent or from which they were received.
The middle term represents a role balance factor, scaling from 1 (completely one-sided exchange) to 2 (perfectly reciprocal exchange). Polygons with no exchange (S+R=0) were assigned a score of zero. This formulation prioritizes polygons that not only have high exchange but also support bidirectional and broadly distributed connectivity with APEIs. The spatial configuration of grid-cell wise *A* can be seen in Ext. Dat. Fig. 5.

CCZ-Wide Connectivity Structure

To assess broad-scale connectivity across the CCZ, we applied a gridded network analysis at 100 × 100 km resolution (Ext. Dat. Fig. 3), following a species-agnostic 'everything is everywhere' framework[22], and assigned each released particle to a grid cell. Each grid cell was treated as a node, and larval fluxes between cells formed directional, weighted edges. Network metrics – including cell-wise out-degree (source strength), in-degree (sink strength), and betweenness centrality (connector role) - were calculated using the 'igraph' package[67], with self-recruitment excluded from structural metrics to avoid inflating node connectivity (but retained in visualisations and summaries). Community detection was performed using the fast-greedy algorithm[68] to delineate clusters of high internal and low external connectivity. These communities represent statistical, not biological, groupings and should not be interpreted as ecological communities in the traditional biological sense (i.e. assemblages of interacting species). Modularity and assortativity were calculated[68,69] to assess network compartmentalisation. Modularity and assortativity values range from -1 to 1, where positive modularity indicates strong internal connectivity within communities and negative or low values suggest weak or diffuse structure. Assortativity reflects whether cells tend to connect with others of similar connectivity, with higher values indicating stronger preference. Community characteristics (size, strength, density) were quantified as the number of cells, total connection

weight (i.e. the number of particles travelling between cells within the community), and the ratio of realised to possible links, respectively[70].

Simulating the impact and recovery of mining

To assess how mining may affect CCZ-wide connectivity, we conducted two complementary simulations:

1. *Mining-origin particle exclusion*: To identify transitional zones - cells that shift community affiliation under future disturbance - we re-ran the community detection analysis using a filtered dataset excluding all particles released from mining contract areas[44]. Each cell's community identity under full and disturbed scenarios was compared, and cells with differing assignments were classified as transitional. These zones lie at the boundaries of semi-isolated dispersal communities and act as ecological bridges; their protection helps preserve regional cohesion and maintain gene flow in the face of mining pressure. Cells in the grid were given a binary status (T_i) variable set to 1 for transitional zones and 0 otherwise.

2. *Larval supply to mining regions:* we traced the origin cells of all particles that settled within mining zones. This analysis identified which non mining regions supply larvae to potentially impacted areas, highlighting critical contributors to potential post-mining recovery and resilience. For each 100 × 100 km polygon in the CCZ we calculated the number of particles that reached mining areas, the number of mining areas reached, and the proportion of particles released from that polygon that reached a mining zone. To derive a composite mining replenishment score (M_i: Ext. Dat. Fig. 6) for each polygon, we applied Principal Component Analysis (PCA) to the three metrics. PCA identifies the dominant axis of variation across polygons and combines the metrics into a single score without relying on arbitrary weights. The first principal component (PC1), which captured the majority of variance in the data, was used as the replenishment score. This approach allowed us to objectively rank polygons by their overall importance in replenishing mining areas, integrating total contribution, spatial reach, and delivery efficiency into a single continuous metric.

Identifying scenario-stable connectivity hotspots

To identify grid cells that consistently contribute to CCZ-wide connectivity, both now and under future mining scenarios, we developed a scenario-stable connectivity score. This metric integrates two core structural indicators from the gridded network analysis: out-degree (representing source strength) and node betweenness (indicating stepping-stone importance). Each metric was calculated under two scenarios: one using the full particle dataset (including particles released from all areas), and one excluding particles originating within mining contract zones[44]. All four metrics (two per scenario) were min–max normalised independently to account for differences in network structure between scenarios and to ensure equal weighting. Since the absolute magnitude and ecological importance of each metric (e.g. source strength vs. stepping-stone role) are not directly comparable or known, normalisation allowed each to contribute proportionately to the composite score[22]. The final scenario-stable score (S_i) for each cell was calculated as the mean of these normalised values. This approach prioritises cells that remain important larval contributors and connectors even under potential mining-induced source loss.

Algorithm for APEI Network Optimization

To guide the strategic expansion of the APEI network, we developed a spatial prioritisation framework to identify high-impact areas for protection, building on the Connectivity Importance Index (CCI) developed by James et al.[22]. Our approach targets locations that consistently support network function and resilience, offering robust, science-based guidance for spatial planning.

An Integrated Connectivity Value (*ICV:* Ext. Dat. Fig. 7) for each 100 × 100 km polygon in the CCZ grid was calculated from the APEI support score (A_i), the mining replenishment score (M_i), and the scenario-stable connectivity score (S_i) with a transitional status indicator (T_i) following:

$$ICV_i = \frac{1}{4}\left(\frac{A_i - A_{min}}{A_{max} - A_{min}} + \frac{M_i - M_{min}}{M_{max} - M_{min}} + \frac{S_i - S_{min}}{S_{max} - S_{min}} + T_i\right)$$

We applied equal weights to the four components of the ICV score to ensure that no single criterion dominates the outcome. This approach reflects the multi-objective nature of the prioritization process, where ecological function, management relevance, and structural shifts are considered equally important. Assigning equal weight avoids introducing subjective bias toward any one metric and aligns with precautionary, inclusive conservation planning principles. To justify this approach, we assessed pairwise correlations among the components. All correlation coefficients were below 0.5, and the fourth component (reflecting community reassignments) was particularly weakly correlated with the others ($r < 0.1$ in all cases). This confirms that the components contribute complementary information and supports their treatment as distinct and equally weighted in the final score.

Finally, we developed an iterative spatial algorithm to identify the smallest set of additional grid cells needed to connect the existing APEI network via observed larval dispersal paths. First, we ranked all non-APEI polygons by their Integrated Connectivity Value (ICV) and incrementally included them until all APEIs were connected through mutual dispersal links, ensuring ecological cohesion via high-value areas. We then refined this network using a graph-theoretic optimization approach adapted from Steiner tree methods[71], which aims to connect terminal nodes through the minimal total network cost. In our adaptation, we built an undirected graph using only reciprocal exchange links that met a particle flow threshold (of 1000 particles) and computed the minimal set of paths required to connect all APEIs. Unlike classical Steiner tree formulations, which minimize geometric or cost distances, our weighting favoured dispersal routes with strong and symmetrical larval exchange. This ensured biological relevance while reducing the number of added polygons to the minimum necessary to maintain functional network integrity.

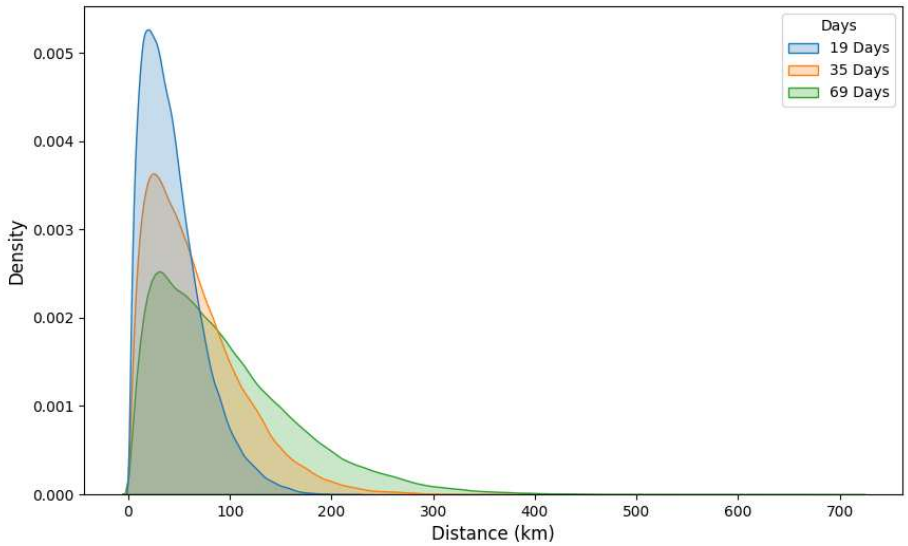
References (Methods)

42. Natural Earth. *1:10m Physical Vectors*. Available at: https://www.naturalearthdata.com/ (2022).
43. Elson, P. et al. Cartopy: a cartographic Python library with a Matplotlib interface. *J. Open Source Softw.* **7**, 3821 (2022).
44. International Seabed Authority. *The geographical limits of the Clarion-Clipperton Zone management area, exploration areas, reserved areas and areas of particular environmental interest (APEIs)* (ISBA/17/LTC/7, ISBA/18/C/22, ISBA/26/C/58, ISBA/26/C/43). Available at: https://www.isa.org.jm/exploration-contracts/maps/ (2023). Accessed 27 Sept 2024.
45. Cummings, J. A. & Smedstad, O. M. Variational data assimilation for the global ocean. in *Data Assimilation for Atmospheric, Oceanic and Hydrologic Applications* Vol. II (eds. Park, S. & Xu, L.) 303–343. Springer, Berlin, Heidelberg. (2013).
46. GEBCO Compilation Group. GEBCO 2020 Grid – A continuous terrain model of the global oceans and land. Version 2020.1. *British Oceanographic Data Centre* https://doi.org/10.5285/49c1c2d4-c1c7-6a6f-e053-6c86abc0c7a8 (2020).
47. Chassignet, E.P. *et al.* The HYCOM (hybrid coordinate ocean model) data assimilative system. *J. Mar. Sys.*, **65**(1-4), 60-83. (2007).
48. Aleynik, D., Inall, M. E., Dale, A. & Vink, A. Impact of remotely generated eddies on plume dispersion at abyssal mining sites in the Pacific. *Sci. Rep.* **7**, 16959 (2017).
49. Lange, M. & van Sebille, E. Parcels v0. 9: prototyping a Lagrangian ocean analysis framework for the petascale age. *Geosci. Mod. Dev.*, **10**(11), 4175-4186.
50. NOAA Climate.gov. February 2019 El Niño arrives. *NOAA Climate.gov* https://www.climate.gov/news-features/blogs/enso/february-2019-el-ni%C3%B1o-arrives (2019).
51. NOAA CPC. ENSO Diagnostic Discussion – July 2019. *NOAA Climate Prediction Center* https://www.cpc.ncep.noaa.gov/products/analysis_monitoring/enso_disc_jul2019/ensodisc.shtml (2019).
52. NOAA Climate.gov. January 2023 La Niña update: and the ENSO Blog investigates, Part 2. *NOAA Climate.gov* https://www.climate.gov/news-features/blogs/enso/january-2023-la-nina-update-and-enso-blog-investigates-part-2 (2023).
53. NOAA Climate.gov. July 2023 El Niño update: learning the steps. *NOAA Climate.gov* https://www.climate.gov/news-features/blogs/enso/july-2023-el-nino-update-learning-steps (2023).
54. James, M. K**.** *et al.* Reverse engineering field-derived vertical distribution profiles to infer larval swimming behaviors. *Proc. Natl Acad. Sci. USA* **116**, 11818–11823 (2019).
55. James, M. K. *et al.* Assessing the influence of behavioural parameterisation on the dispersal of larvae in marine systems. *Ecol. Model.* **476**, 110252 (2023).
56. Gamoyo, M., Obura, D. & Reason, C. J. C. Estimating connectivity through larval dispersal in the Western Indian Ocean. *J. Geophys. Res. Biogeosci.* **124**, 2446–2459 (2019).
57. Smagorinsky, J. General circulation experiments with the primitive equations: I. The basic experiment. *Mon. Weath. Rev.* **91**(3), 99-164 (1963).
58. Ross, O.N. & Sharples, J.Recipe for 1-D Lagrangian particle tracking models in space-varying diffusivity. *Limn. Oce: Meth*, ***2***(9), 289-302 (2004).
59. Courant, R., Friedrichs, K. & Lewy, H**.** On the partial difference equations of mathematical physics. *IBM J. Res. Dev.* **11**, 215–234 (1967).

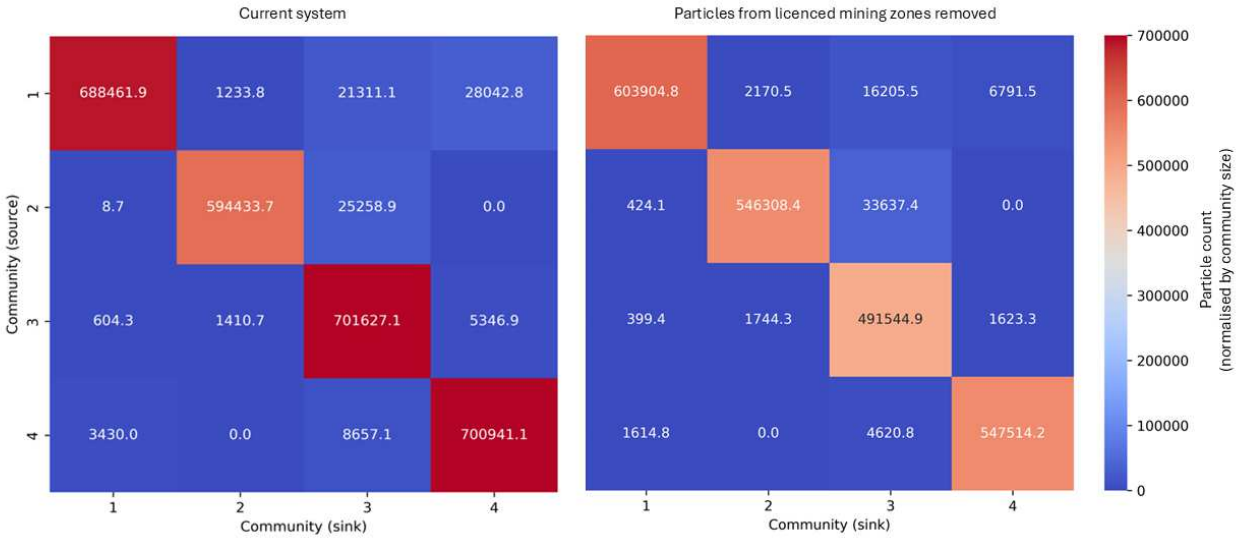
60. Ross, R. E., Nimmo-Smith, W. A. M. & Howell, K. L. Increasing the depth of current understanding: sensitivity testing of deep-sea larval dispersal models for ecologists. *PLoS One* **11**, e0161220 (2016).
61. Swearer, S. E., Treml, E. A. & Shima, J. S. A review of biophysical models of marine larval dispersal. In *Oceanography and Marine Biology: An Annual Review* (eds. Hughes, R. N., Hughes, D. J. & Smith, I. P.) **57**, 325–356. CRC Press (2019).
62. Virtanen, P *et al.* SciPy 1.0: fundamental algorithms for scientific computing in Python. *Nature methods*, ***17***(3), 261-272 (2020).
63. Simons, R.D., Siegel, D.A. & Brown, K.S. Model sensitivity and robustness in the estimation of larval transport: a study of particle tracking parameters. *J. Mar. Sys.*, *119*, 19-29 (2013)
64. Jaccard, P. Étude comparative de la distribution florale dans une portion des Alpes et du Jura. *Bull. Soc. Vaud. Sci. Nat.* **37**, 547–579 (1901).
65. Cohen, J. A Coefficient of Agreement for Nominal Scales. *Edu. Psych. Meas.*, 20(1), 37-46 (1960).
66. Ramiadantsoa, T., Ovaskainen, O., Rybicki, J. & Hanski, I. Large-scale habitat corridors for biodiversity conservation: A forest corridor in Madagascar. *PLoS ONE* **10**, e0132126 (2015).
67. Csardi, G. & Nepusz, T. The igraph software package for complex network research. *InterJournal Complex Systems*, 1695 (2006). Available at: https://igraph.org
68. Clauset, A., Newman, M. E. J. & Moore, C. Finding community structure in very large networks. *Phys. Rev. E* **70**, 066111 (2004).
69. Pearson, K. Mathematical contributions to the theory of evolution. III. Regression, heredity, and panmixia. *Philos. Trans. R. Soc. Lond. A* **187**, 253–318 (1896).
70. Lancichinetti, A. & Fortunato, S. Community detection algorithms: a comparative analysis. *Physical review E*, 80(5), 056117 (2009).
71. Hwang, F.K. & Richards, D.S. Steiner tree problems. *Networks*, 22(1), 55-89 (1992).

Extended Data

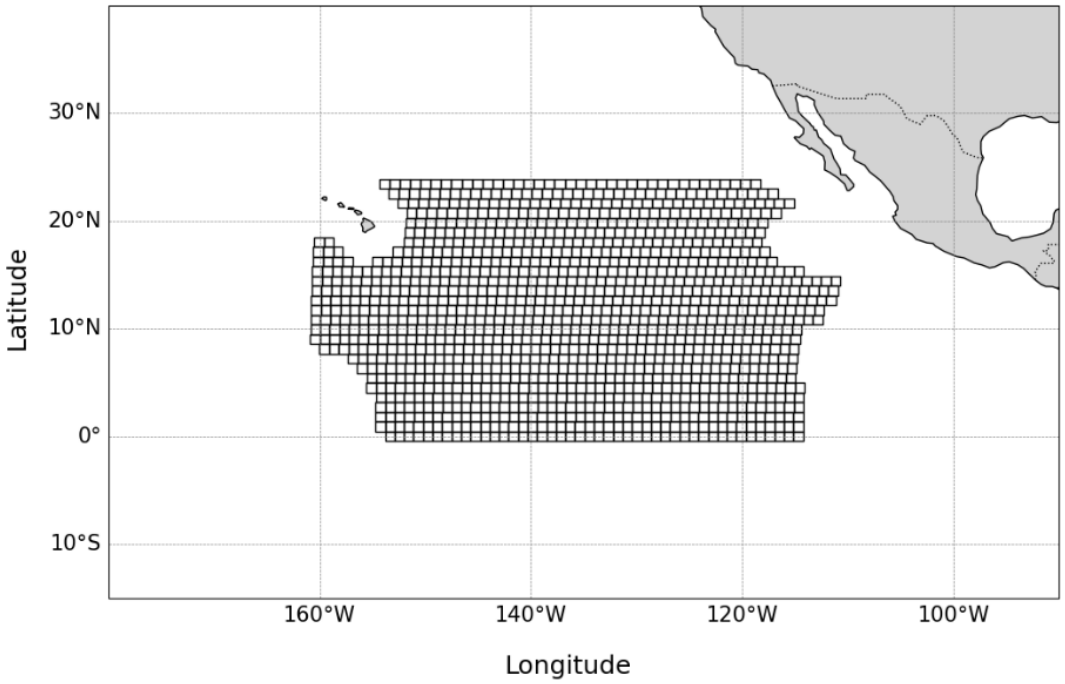
Figures



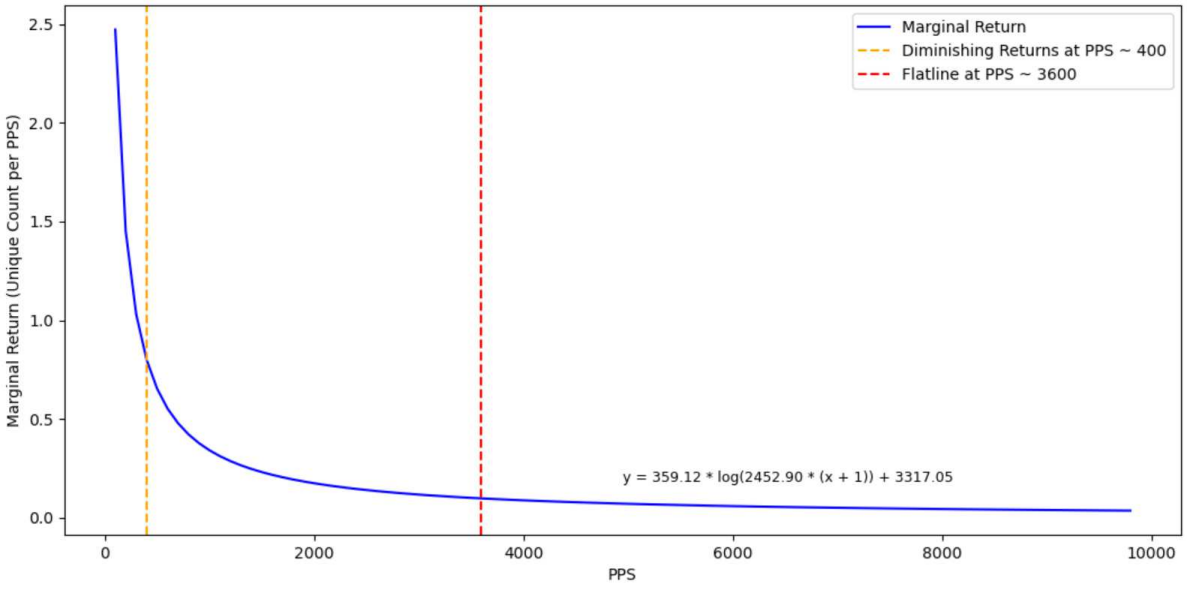
Extended Data Figure 1: Density distributions of particle dispersal distances for three simulation durations (PLDs): 19 days (blue), 35 days (orange), and 69 days (green). Particle retention within the CCZ was extremely high, with only 0.84% of particles settling outside the CCZ boundaries after 69 days of tracking, and only marginally increasing with dispersal duration (19 days: 0.23%; 35 days 0.43%). As PLD increased, the median distance travelled by the particles also increased from 37.74km at 19 days PLD to 80.79km at 69 days PLD (35 days: 55.45km). Variability in dispersal distance also increased with increasing PLD. Maximum dispersal distances increased substantially, with some particles travelling up to 553km in 69 days, however median distances travelled remained below 100km, irrespective of dispersion time.



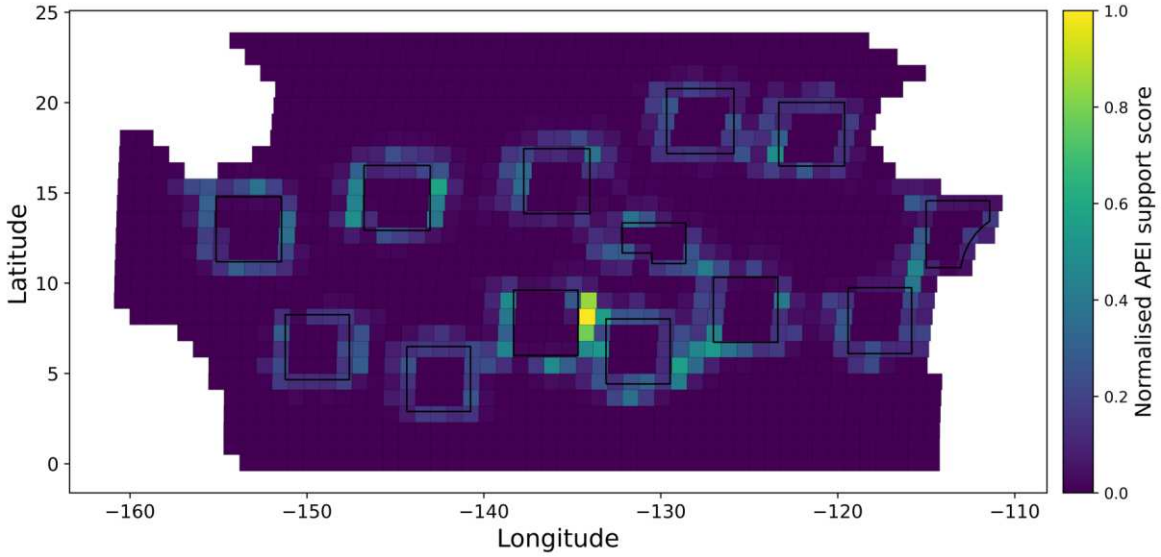
Extended Data Figure 2: Community-level connectivity matrices showing the volume of larval exchange between communities, normalised by the sizes of source and sink communities. ***Left:*** current system ***Right:*** particles of mining area origin removed. Diagonal values indicate self-retention within each community, while off-diagonal elements represent cross-community exchange. Higher values (red) indicate stronger connectivity.



Extended Data Figure 3: 100 × 100km grid cells (N = 1,225) covering the area of the Clarion-Clipperton Zone (CCZ).



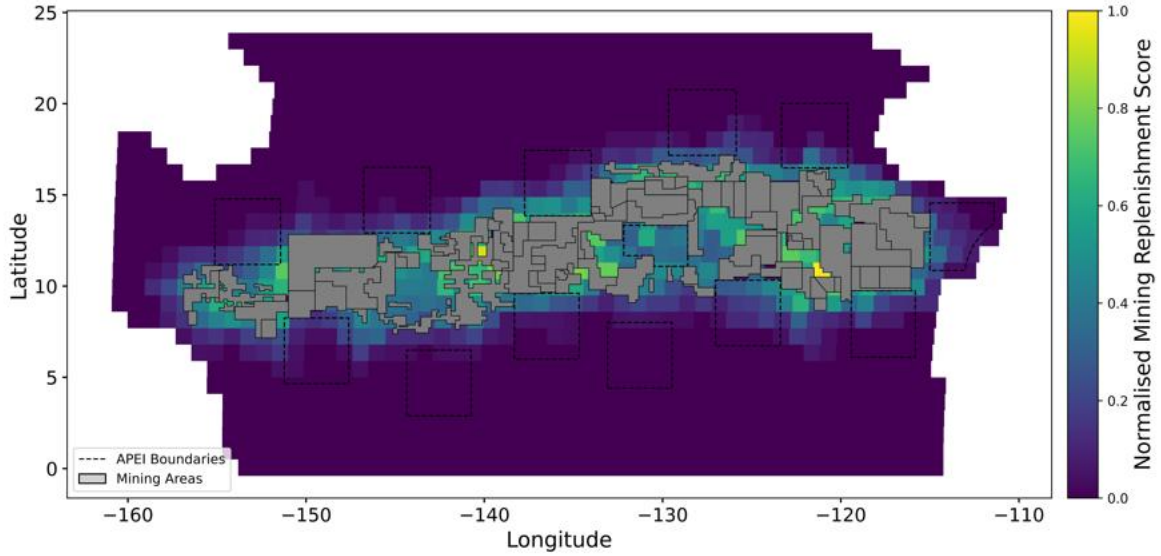
Extended Data Figure 4: Marginal returns (unique count increase per additional Particles Per Site (PPS)) as a function of PPS. The curve was fitted using a logarithmic model to best represent diminishing returns in unique counts as PPS increases. Orange vertical line marks the point of diminishing returns where the marginal return falls below 1, and the red vertical line denotes the point at which the marginal return is less than 0.1.



748

749 **Extended Data Figure 5**: Normalised APEI support scores (*A*) across the CCZ. Grid cells (100 × 100 km) are coloured
750 by their support for larval connectivity to existing APEIs (dashed black outlines). Higher scores (yellow) indicate
751 stronger support for network connectivity.

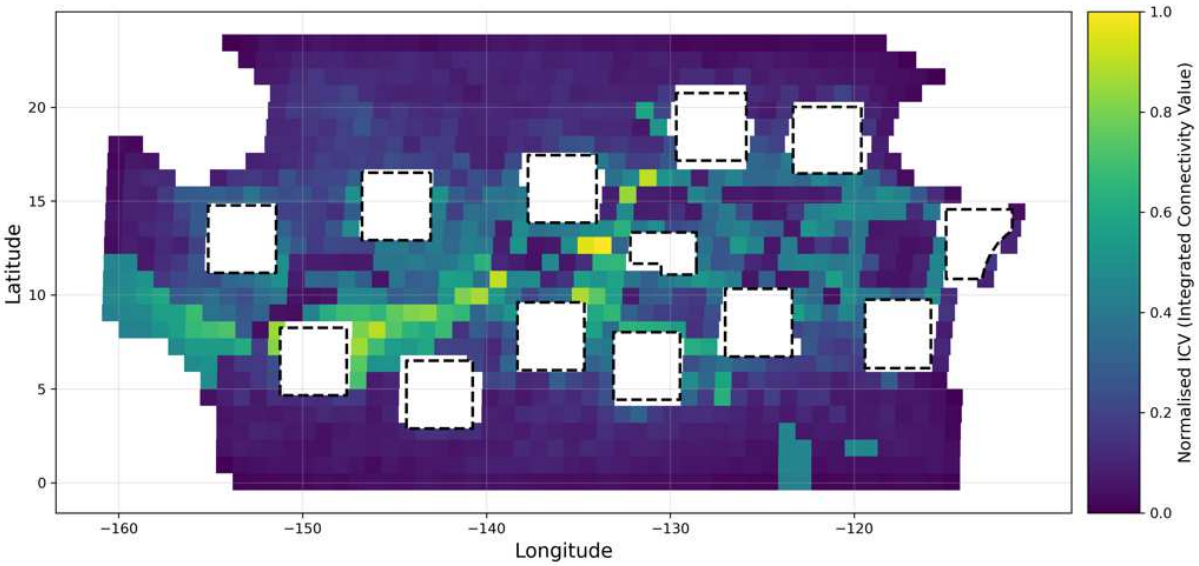
752



753

754 **Extended Data Figure 6**: Normalised mining replenishment scores (*M*) across the *CCZ.* Grid cells (100 × 100 km) are
755 coloured by their composite contribution to larval supply into mining areas (grey polygons), based on total flux, spatial
756 reach, and delivery efficiency. Dashed black outlines show APEI boundaries.

757



Extended Data Figure 7: Integrated Connectivity Values (ICV) across the CCZ. Grid cells (100 × 100 km) are coloured by their normalised ICV, combining APEI support, mining replenishment potential, scenario stability, and community transition status. Dashed black outlines indicate existing APEI boundaries.

Tables

Extended Data Table 1: El Niño–Southern Oscillation (ENSO) Phase Classification for particle release dates (January and July 2019 and 2023), based on referenced NOAA Reports.

Date	***ENSO Phase***	***Notes***
January 2019	*El Niño (weak)*	*El Niño conditions developing; officially declared in Feb 2019*[50]
July 2019	*El Niño (weak; ending)*	*Weak El Niño still present, but transitioning to neutral*[51]
January 2023	*La Niña (weakening)*	*Ongoing La Niña, with neutral conditions expected in the coming months*[52]
July 2023	*El Niño (developing)*	*El Niño conditions established: string event expected by Winter*[53]

Extended Data Table 2: Summary of simulation parameters used in the larval dispersal model.

Simulation ID	*Release Month*	*Year*	*Pelagic Larval Duration (PLD) (days)*	*Particles Released*
S1	*January*	*2013*	*19*	*68,140,992*
S2	*January*	*2013*	*35*	*68,140,992*
S3	*January*	*2013*	*69*	*68,140,992*
S4	*July*	*2013*	*19*	*68,140,992*
S5	*July*	*2013*	*35*	*68,140,992*
S6	*July*	*2013*	*69*	*68,140,992*
S7	*January*	*2019*	*19*	*68,140,992*
S8	*January*	*2019*	*35*	*68,140,992*
S9	*January*	*2019*	*69*	*68,140,992*
S10	*July*	*2019*	*19*	*68,140,992*
S11	*July*	*2019*	*35*	*68,140,992*
S12	*July*	*2019*	*69*	*68,140,992*
Total				***817,691,904***

Extended Data Table 3: Jaccard distances, Cohen's Kappa and permutations test results comparing larval connectivity across Seasons (January Vs. July) and years (2019 vs. 2023).

Comparison	*Jaccard Distance (dj)*	*Cohen's Kappa statistic*	*Jaccard Permutation (n=9999) P-value*
January 2019 vs. July 2019	0.56	-0.38	<0.001***
January 2023 vs. July 2023	0.54	-0.36	<0.001***
January 2019 vs. January 2023	0.48	-0.32	<0.001***
July 2019 vs. July 2023	0.5	-0.28	<0.001***